Inorg. Chem. **2006**, *45*, 11008–11018

Guanidinate-Stabilized Monomeric Hafnium Amide Complexes as Promising Precursors for MOCVD of HfO_2

Andrian Milanov,[†] Raghunandan Bhakta,[†] Arne Baunemann,[†] Hans-Werner Becker,[‡] Reji Thomas,[§] Peter Ehrhart,[§] Manuela Winter,[†] and Anjana Devi*,[†]

Inorganic Materials Chemistry Group, Lehrstuhl für Anorganische Chemie II, Ruhr-University Bochum, D-44780 Bochum, Germany, Lehrstuhl für Experimentalphysik III, Ruhr-University Bochum, D-44780 Bochum, Germany, and IFF-Institut für Festkörperforschung and CNI-Center for Nanoelectronic Systems for Information Technology, Forschungszentrum Jülich, D-52425 Jülich, Germany

Received June 13, 2006

Novel guanidinato complexes of hafnium $[Hf\{\eta^2\text{-}(^iPrN)_2CNR_2\}_2(NR_2)_2]$ ($R_2 = Et_2$, **1**; Et, Me, **2**; Me_2, **3**), synthesized by insertion reactions of *N,N′*-diisopropylcarbodiimide into the M–N bonds of homologous hafnium amide complexes **1**–**3** and $\{[\mu_2\text{-}NC(NMe_2)_2][NC(NMe_2)_2]_2HfCl\}_2$ (**4**) using a salt metathesis reaction, are reported. Single-crystal X-ray diffraction analysis revealed that compounds **1**–**3** were monomers, while compound **4** was found to be a dimer. The observed fluxional behavior of compounds **1**–**3** was studied in detail using variable-temperature and two-dimensional NMR techniques. The thermal characteristics of compounds **1**–**3** seem promising for HfO_2 thin films by vapor deposition techniques. Metal–organic chemical vapor deposition experiments with compound **2** as the precursor resulted in smooth, uniform, and stoichiometric HfO_2 thin films at relatively low deposition temperatures. The basic properties of HfO_2 thin films were characterized in some detail.

Introduction

The scaling down of semiconductor device dimensions has led to the exploration of new high-*k* dielectrics due to the high leakage currents observed with the conventionally used SiO_2. High-permittivity oxides like HfO_2 and ZrO_2 are currently being investigated as alternative materials for conventional SiO_2-based gate oxides in complementary metal oxide semiconductor devices.[1,2] In addition, these oxide materials have numerous other applications such as optical fibers, sensors, thermal barrier coatings, waveguides, etc.[3] These potential applications have enhanced the research activities related to the growth of high-quality thin films of these materials by several techniques, which include sputtering, molecular beam epitaxy, chemical vapor deposition (CVD), etc.[4] Among the various techniques that are available for thin film growth, metal−organic CVD (MOCVD) and the related technique, namely, atomic layer deposition (ALD), have emerged as effective techniques for the growth of thin films, offering the potential for large area deposition, good composition control, and film uniformity as well as excellent conformal coverage on nonplanar device geometries. The essential requirement for a successful vapor deposition process such as MOCVD or ALD is the availability of suitable precursors possessing appropriate thermal and physical properties. To date, Hf-based (HfO_2, HfSiON, and HfSiN) dielectrics are considered to be the most promising materials to replace SiO_2 or SiON gate dielectrics. Therefore, recent research interests have focused on the development of new or improved Hf precursors for MOCVD and ALD processes. Many precursors have been employed for the growth of HfO_2

* To whom correspondence should be addressed. E-mail: anjana.devi@rub.de.
[†] Lehrstuhl für Anorganische Chemie II, Ruhr-University Bochum.
[‡] Lehrstuhl für Experimentalphysik III, Ruhr-University Bochum.
[§] IFF-Institut für Festkörperforschung and CNI-Center for Nanoelectronic Systems for Information Technology.

(1) Semiconductor Industry Association. *International Technology Roadmap for Semiconductors (ITRS)*, 2005. http://www.itrs.net/Common/2005ITRS/Home2005.htm
(2) Wilk, G. D.; Wallace, R. M; Anthony, J. M. *J. Appl. Phys.* **2001**, *89*, 5253.
(3) (a) Kukli, K.; Ritala, M.; Sajavaara, T.; Keinonen, J.; Leskela, M. *Chem. Vap. Deposition* **2002**, *8*, 199. (b) Cameron, M. A.; George, S. M. *Thin Solid Films* **1999**, *348*, 90. (c) Sayer, M.; Sreenivas, K. *Science* **1990**, *247*, 1056.
(4) (a) Seo, J. W.; Dieker, Ch.; Locquet, J.-P.; Mavrou, G.; Dimoulas, A. *Appl. Phys. Lett.* **2005**, *87* (22), 221906. (b) Kuo, C. T.; Kwor, R.; Jones, K. M. *Thin Solid Films* **1992**, *213* (2), 257. (c) Park, J.; Park, B. K.; Cho, M.; Hwang, C. S.; Oh, K.; Yang, D. Y. *J. Electrochem. Soc.* **2002**, *149* (1), G89.

10.1021/ic061056i CCC: $33.50
Published on Web 12/01/2006

thin films by CVD or ALD.[5,6] Among them, the homoleptic precursors such as metal halogenides, β-diketonates, nitrates, alkoxides, and alkylamides have been most frequently used.[7−10] Unfortunately, there are certain drawbacks associated with existing precursors, such as high evaporation and deposition temperatures, carbon and halogen incorporation in the films, and high air and moisture sensitivity.

The concept of engineering of the existing class of precursors for, e.g., use of different ancillary ligands in combination with hafnium and zirconium alkoxides, showed some promise in terms of improved thermal properties, moisture sensitivity, etc.[11−13] Another class of compounds that have drawn much attention as precursors are the metal alkylamides [$M(NR_2)_4$], which show considerable potential for metal oxide growth by MOCVD or ALD.[14] These compounds do not possess direct M−C bonds. In the process, the carbon contamination in the resulting films could be minimized. The employment of metal alkylamides such as [$Hf(NEt_2)_4$] as precursors in combination with O_2 or N_2O has resulted in high-quality thin films of HfO_2 by MOCVD or ALD.[14−19] However, a potential drawback associated with metal alkylamides is their high sensitivity toward air and moisture, which can lead to difficulties in handling and storage. In an attempt to develop improved precursors of Hf, we were keen to engineer the amide class of compounds.

Scheme 1. 1,1,3,3-Tetramethylguanidine (Left) and *N*,*N*′-Dialkyl-2-(dialkylamido)guanidinate Ligand (Right)

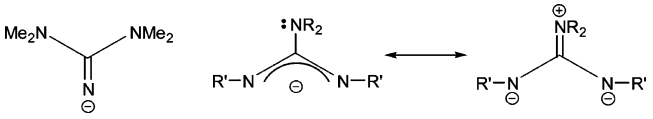

Our efforts in using malonates as chelating ligands in combination with metal alkylamides resulted in a new class of mixed amido/malonato complexes.[20,21] These six-coordinate complexes with mixed O/N ligand spheres are much less sensitive than the parent alkylamides and show promise for HfO_2 thin film deposition, by both thermal CVD and liquid-injection MOCVD (LI-MOCVD) processes. Following a similar approach to tailor amide-based complexes, we attempted the synthesis of all-N-coordinated complexes of Hf using chelating ligands as precursors, which could serve as precursors for HfO_2 thin film growth.

Recently, there has been growing interest in another class of bidentate chelating ligands, namely, *N*,*N*′-dialkyl-2-alkylamidinates, which bind the metal center through M−N bonding. The amidinates $[(R'N)_2CR]^-$ are known to be versatile ligands in organometallic chemistry, co-coordinating to a wide range of metals, and are found to be suitable for metal oxide deposition by ALD and CVD techniques.[22,23] Recent reports have shown that the related guanidinate anion $[(R'N)_2CNR_2]^-$ can impart a similar coordination environment while offering increased stability due to the possibility of the additional zwitterionic resonance structure (Scheme 1).[24] Moreover, guanidinate ligands provide tuneability in terms of steric and electronic properties, by variation of the substituents R and R′ and, hence, are used extensively for many elements across the periodic table.[24−36] As a part of our research interest in the precursor chemistry of Hf, we undertook the synthesis of a range of hafnium amides with a stabilizing guanidinate ligand system.

(5) (a) Balog, M.; Schieber, M.; Patai, S.; Michman, M. *J. Cryst. Growth* **1972**, *17*, 298. (b) Williams, P. A.; Roberts, J. L.; Jones, A. C.; Chalker, P. R.; Tobin, N. L.; Bickley, J. F.; Davies, H. O.; Smith, L. M.; Leedham, T. J. *Chem. Vap. Deposition* **2002**, *8* (4), 163.

(6) (a) Aarik, J.; Sundqvist, J.; Aidla, A.; Lu, J.; Sajavaara, T.; Kukli, K.; Harsta, A. *Thin Solid Films* **2002**, *418* (2), 69. (b) Potter, R. J.; Chalker, P. R.; Manning, T. D.; Aspinall, H. C.; Loo, Y. F.; Jones, A. C.; Smith, L. M.; Critchlow, G. W.; Schumacher, M. *Chem. Vap. Deposition* **2005**, *11* (3), 159. (c) Niinistö, J.; Putkonen, M.; Niinistö, L.; Stoll, S. L.; Kukli, K.; Sajavaara, T.; Ritala, M.; Leskela, M. *J. Mater. Chem.* **2005**, *15* (23), 2271.

(7) (a) Pierson, H. O. *Handbook of Chemical Vapor Deposition (CVD)*; William Andrew Publishing: LLC Norwich, New York, 1999. (b) Choi, K. J.; Shin, W. C.; Yoon, S. G. *J. Electrochem. Soc.* **2002**, *F18*, 149. (c) Park, J.; Park, B. K.; Cho, M.; Hwang, C. H.; Oh, K.; Yang, D. Y. *J. Electrochem. Soc.* **2002**, *149* (1), 89.

(8) Jones, A. C. Recent Developments in the MOCVD of Electronic Materials. *Adv. Mater. Opt. Electron.* **2000**, *10*.

(9) Conley, J. J. F.; Ono, Y.; Zhuang, W.; Tweet, D. J.; Gao, W.; Mohammed, S. K.; Solanki, R. *Electrochem. Solid State Lett.* **2002**, *5*, C57.

(10) Gordon, R. G.; Becker, J.; Hausmann, D.; Suh, S. *Chem. Mater.* **2001**, *13*, 2463.

(11) Baunemann, A.; Thomas, R.; Becker, R.; Winter, M.; Fischer, R. A.; Ehrhart, P.; Waser, R.; Devi, A. *Chem. Commun.* **2004**, 1610.

(12) Patil, U.; Winter, M.; Becker, H.-W.; Devi, A. *J. Mater. Chem.* **2003**, *13*, 2177.

(13) Patil, U.; Thomas, R.; Milanov, A.; Bhakta, R.; Ehrhart, P.; Waser, R.; Becker, R.; Becker, H.-W.; Winter, M.; Merz, K.; Fischer, R. A.; Devi, A. *Chem. Vap. Deposition* **2006**, *12*, 172.

(14) (a) Ohshita, Y.; Ogura, A.; Hoshino, A.; Hiiro, S.; Suzuki, T.; Machida, H. *Thin Solid Films* **2002**, *406*, 215. (b) Hausmann, D. M.; Kim, E.; Becker, J.; Gordon, R. J. *Chem. Mater.* **2002**, *14*, 4350. (c) Bastiani, A.; Battiston, G. A.; Gerbasi, R.; Porchia, M.; Daolio, S. *J. Phys. IV* **1995**, *5*, C-525.

(15) Hausmann, D. M.; Kim, E.; Becker, J.; Gordon, R. G. *Chem. Mater.* **2002**, *14*, 4350.

(16) Deshpande, A.; Inman, R.; Jursich, G.; Takoudis, C. *J. Vac. Sci. Technol.* **2004**, *A22* (5), 2035.

(17) Machida, H.; Hoshino, A.; Suzuki, T.; Ogura, A.; Ohshita, Y. *J. Cryst. Growth* **2002**, *237*−*239*, 586.

(18) Takahashi, K.; Nakayama, M.; Yokoyama, S.; Kimura, T.; Tokumitsu, E.; Funakubo, H. *Appl. Surf. Sci.* **2003**, *216*, 296.

(19) Lee, M.; Lu, Z.-H.; Ng, W.-T.; Landheer, D.; Wu, X.; Moisa, S. *Appl. Phys. Lett.* **2003**, *83* (13), 2638.

(20) Milanov, A.; Bhakta, R.; Thomas, R.; Erhart, P.; Winter, M.; Waser, R.; Devi, A. *J. Mater. Chem.* **2006**, *16*, 437.

(21) Thomas, R.; Milanov, A.; Bhakta, R.; Patil, U.; Winter, M.; Ehrhart, P.; Waser, R.; Devi, A. *Chem. Vap. Deposition* **2006**, *12*, 295.

(22) Lim, B. S.; Rahtu, A.; Gordon, R. G. *Nature* **2003**, *2*, 749.

(23) Lim, B. S.; Rahtu, A.; Park, J.-S.; Gordon, R. G. *Inorg. Chem.* **2003**, *42*, 7951.

(24) Bailey, P. J.; Pace, S. *Coord. Chem. Rev.* **2001**, *214*, 91.

(25) Chandra, G.; Jenkins, A. D.; Lappert, M. F.; Srivastava, R. C. *J. Chem. Soc. A* **1970**, 2550.

(26) Aeilts, S. L.; Coles, M. P.; Swenson, D. C.; Jordan, R. F.; Young, V. G. J. *Organometallics* **1998**, *17*, 3265.

(27) Decams, J. M.; Hubert-Pfalzgraf, L. G.; Vaissermann, J. *Polyhedron* **1999**, *18*, 2885.

(28) Tin, M. K. T.; Yap, G. P. A.; Richeson, D. S. *Inorg. Chem.* **1999**, *38*, 998.

(29) Tin, M. K. T.; Thirupathi, N.; Yap, G. P. A.; Richeson, D. S. *J. Chem. Soc., Dalton Trans.* **1999**, 2947.

(30) Wood, D.; Yap, G. P. A.; Richeson, D. S. *Inorg. Chem.* **1999**, *38*, 5788.

(31) Bailey, P. J.; Grant, K. J.; Mitchell, L. A.; Pace, S.; Parkin, A.; Parsons, S. *J. Chem. Soc., Dalton Trans.* **2000**, 1887.

(32) Duncan, A. P.; Mullins, S. M.; Arnold, J.; Bergmann, R. G. *Organometallics* **2001**, *20*, 1808.

(33) Lu, Z.; Yap, G. P. A.; Richeson, D. S. *Organometallics* **2001**, *20*, 706.

(34) Cotton, F. A.; Daniels, L. M.; Murillo, C. A.; Timmons, D. J.; Wilkinson, C. C. *J. Am. Chem. Soc.* **2002**, *124*, 9249.

(35) Ong, T.-G.; Wood, D.; Yap, G. P. A.; Richeson, D. S. *Organometallics* **2002**, *21*, 1.

(36) Baunemann, A.; Rische, D.; Milanov, A.; Kim, Y.; Winter, M.; Gemel, C.; Fischer, R. A. *Dalton Trans.* **2005**, 3051.

Table 1. Crystallographic Data for Compounds **1**−**4**

compound	**1**	**2**	**3**	**4**
empirical formula	$C_{30}H_{68}HfN_8$	$C_{26}H_{60}HfN_8$	$C_{22}H_{52}HfN_8$	$C_{30}H_{72}Cl_2Hf_2N_{18}$
fw	719.41	663.31	607.196	1112.94
cryst syst	monoclinic	orthorhombic	monoclinic	triclinic
space group	*P*2(1)/*c*	*Pbca*	*C*2/*c*	$P\bar{1}$
Z	8	8	4	1
a (Å)	10.3775(13)	10.8082(5)	19.8714(13)	10.3253(10)
b (Å)	38.724(5)	17.5942(10)	29.6787(13)	11.3293(11)
c (Å)	18.244(2)	33.6626(19)	17.5709(8)	12.1396(12)
β (deg)	95.873(10)	90	116.313(6)	112.46(2)
V (Å^3)	7293.1(16)	6401.3(6)	9288.9(8)	1140.60(19)
d_{calc} (g/cm^3)	1.310	1.377	1.364	1.620
μ (mm^{-1})	2.890	3.286	3.394	4.708
R1[a]	0.0762	0.0998	0.0454	0.0413
wR2[b]	0.1642	0.1568	0.0503	0.0945

[a] $R1 = \sum||F_o| - |F_c||/\sum|F_o|$. [b] $wR2 = \{\sum[w(F_o^2 - F_c^2)^2]\}/\{\sum[w(F_o^2)^2]\}^{1/2}$.

The bidentate chelating effect of the guanidinate ligands is expected to enhance the thermal/chemical stability of the resulting metal complexes and thus make them suitable precursors for the MOCVD and ALD of HfO_2. Furthermore, it has been proposed that donation of the lone pair from the dialkylamido group into the ligand could result in metal complexes being electron-rich when compared to other ligands, such as amidinates.[37] To our knowledge, all-N-coordinated hafnium guanidinate complexes have not been previously reported. We attempted the synthesis and characterization of a new class of bis(dialkylamido)bis[*N*,*N*′-diisopropyl-2-(dialkylamido)guanidinato]hafnium(IV) complexes [Hf{η^2-(^{i}PrN)$_2$CNR$_2$}$_2$(NR$_2$)$_2$] (R$_2$ = Et$_2$, **1**; Et, Me, **2**; Me$_2$, **3**). The guanidinato complexes **1**−**3** were prepared by the insertion of the carbodiimides into the metal−amido linkage. In parallel, the coordination chemistry of all-N Hf complexes, employing salt metathesis reactions using [LiNC(NMe$_2$)$_2$]$_2$, was also investigated. This ligand type has a decreased sterical demand when compared to {[(R′N)$_2$CNR$_2$]$^-$} and is known to bind via the imino N atom in η^1 mode (Scheme 1).[38] Thus, it was proposed that synthesis of a tetrasubstituted Hf complex should be possible. Surprisingly, all attempts to synthesize such a compound by reacting [LiNC(NMe$_2$)$_2$]$_2$ and $HfCl_4$ (salt metathesis reactions) in different molar ratios (4:1 and 3:1) led to the formation of bis[chloro(μ_2-1,1,3,3-tetramethylguanidinato)bis(1,1,3,3-tetramethylguanidinato)hafnium] (**4**).

Apart from testing these complexes as potential precursors for HfO_2 thin film growth, we were keen to explore the possibility of incorporating N into the HfO_2 films, employing precursors that contain preformed M−N bonding. Compared to simple metal oxides for gate oxide application, N-doped metal oxides (by postnitridation) show excellent electrical characteristics such as low-leakage current density and superior thermal stability on silicon.[39,40,46]

In this Article, the synthesis and characterization of four novel hafnium guanidinate complexes (**1**−**4**) as well as the growth and characterization of HfO_2 thin films by MOCVD using [Hf{η^2-(^{i}PrN)$_2$CNEtMe}$_2$(NEtMe)$_2$] (**2**) are presented.

Experimental Section

General Procedures. All reactions and manipulations of air- and moisture-sensitive compounds were performed employing a conventional vacuum/Ar line using standard Schlenk techniques. Sample preparation for further analysis was carried out in an Ar-filled glovebox. All solvents were dried and purified by an MBraun solvent purification system and stored over molecular sieves (4 Å). The NMR solvents were degassed and dried over activated molecular sieves. The hafnium amide starting compounds, namely, [Hf(NEt$_2$)$_4$], [Hf(NEtMe)$_4$], and [Hf(NMe$_2$)$_4$] were synthesized, following modified literature procedures,[41] whereas *N*,*N*′-diisopropylcarbodiimide (Acros) and 1,1,3,3-tetramethylguanidine (Fluka) were used as received.

Physical Measurements. ^{1}H and ^{13}C NMR spectra were recorded on either a Bruker Advance DRX 400 or a Bruker Advance DPX 250 (high- and low-temperature NMR spectroscopy). Elemental analysis was performed by the analytical service of the Chemistry Department (CHNSO Vario EL 1998). Electronic ionization mass spectra were recorded using a Varian MAT spectrometer. Melting points were measured in sealed capillaries under Ar and are uncorrected. The thermal analysis data were obtained on a Seiko TGA/DTA 6300S11 instrument in a N_2 atmosphere (flow rate of 300 mL/min, ambient pressure, heating rate of 5 °C/min).

Synthesis of [Hf{η^2-(^{i}PrN)$_2$CNEt$_2$}$_2$(NEt$_2$)$_2$] (1). To a solution of [Hf(NEt$_2$)$_4$] (1.12 mL, 3 mmol) in 20 mL of hexane was added 2 equiv of *N*,*N*′-diisopropylcarbodiimide (0.94 mL, 6 mmol). During the addition, a slight increase in the temperature was observed. After stirring for 24 h at ambient conditions, the solvent was removed under reduced pressure, which resulted in a white crystalline solid. The obtained solid was extracted into toluene, concentrated, and kept at −30 °C for 24 h to afford colorless crystals. Yield: 2.03 g (94% based on [Hf(NEt$_2$)$_4$]). Mp: 205 °C. Anal. Calcd for $C_{30}H_{68}N_8Hf$: C, 50.09; H, 9.53; N, 15.58. Found: C, 50.15; H,

(37) Mullins, S. M.; Duncan, A. P.; Bergman, R. G.; Arnold, J. *Inorg. Chem.* **2001**, *40*, 6952.
(38) Kretschmer, W. P.; Dijkkuis, C.; Meetsma, A.; Hessen, B.; Teuben, J. H. *Chem. Commun.* **2002**, 608.
(39) Xu, Y.; Musgrave, C. B. *Surf. Sci.* **2005**, *591*, L280.
(40) Tong, K. Y.; Jelencovic, E. V.; Liu, W.; Dai, J. Y. *Microelectron. Eng.* **2006**, *83*, 293.
(41) Bradley, D. C.; Thomas, I. M. *J. Chem. Soc.* **1960**, 3857.
(42) Devi, A.; Rogge, W.; Wohlfart, A.; Hipler, F.; Becker, H.-W.; Fischer, R. A. *Chem. Vap. Deposition* **2000**, *6*, 245.
(43) Littke, A.; Sleiman, N.; Bensimon, C.; Richeson, D. S. *Organometallics* **1999**, *17*, 446.
(44) Mullins, S. M.; Duncan, A. P.; Bergman, R. G.; Arnold, J. *Inorg. Chem.* **2001**, *40*, 6952.
(45) Koterwas, L. A.; Fettinger, J. C.; Sita, L. R. *Organometallics* **1999**, *18*, 4183.
(46) Luo, Q.; Dragomir-Cernatescu, I.; Snyder, R. L.; Rees, W. S., Jr.; Hess, D. W. *J. Electrochem. Soc.* **2006**, *153*, F1.

Scheme 2. Synthesis of Hafnium Guanidinato Complexes **1**−**4**

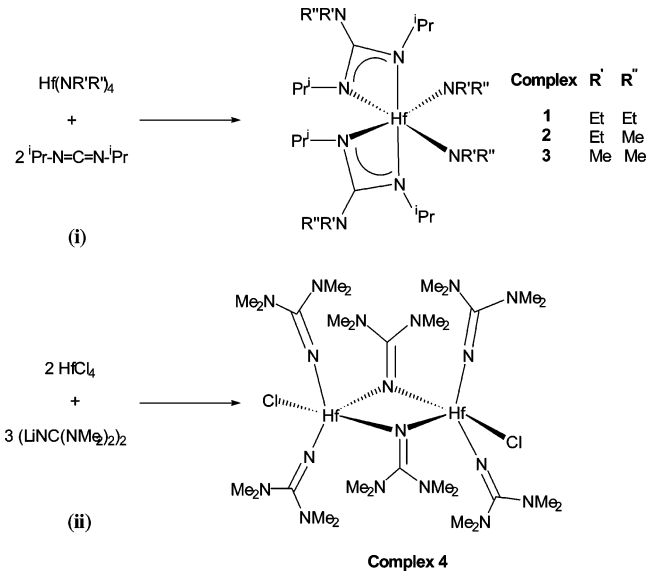

9.74; N, 15.35. ^{1}H NMR (40 °C, 400 MHz, toluene-d_8): δ_H 0.98 (12H, triplet, Hf{(N^{i}Pr)$_2$C(N(CH$_2$C*H*$_3$)$_2$)}), 1.52 (12H, triplet, Hf{N(CH$_2$C*H*$_3$)$_2$}), 1.95, 1.28, 1.40, 1.43 (24H, 4 × doublet, Hf{(N(CH(C*H*$_3$)$_2$))$_2$C(NEt$_2$)}), 2.97−3.05 (8H, multiplet, Hf{(N^{i}Pr)$_2$C(N(C*H*$_2$CH$_3$)$_2$)}), 3.79 (8H, multiplet, Hf{N(C*H*$_2$CH$_3$)$_2$}), 3.87 (4H, septet, Hf{(N(C*H*(CH$_3$)$_2$))$_2$C(NEt$_2$)}). ^{13}C NMR (room temperature, 400 MHz, toluene-d_8): δ_C 14.35 (Hf{(N^{i}Pr)$_2$C(N(CH$_2$C*H*$_3$)$_2$)}, Hf{N(CH$_2$C*H*$_3$)$_2$}), 24.45, 25.69, 25.94, 26.43 (Hf{(N(CH(C*H*$_3$)$_2$))$_2$C(NEt$_2$)}), 42.55 (Hf{(N^{i}Pr)$_2$C(N(C*H*$_2$CH3)$_2$)}, Hf{N(C*H*$_2$CH$_3$)$_2$}), 47.27, 47.72 (Hf{(N(C*H*(CH$_3$)$_2$))$_2$C(NEt$_2$)}), 171.46 (Hf{(N^{i}Pr)$_2$C(N(CH$_2$CH$_3$)$_2$)}).

Synthesis of [Hf{η^2-(iPrN)$_2$CNEtMe}$_2$(NEtMe)$_2$] (2). Following a similar procedure adopted for the synthesis of compound **1**, [Hf(NEtMe)$_4$] (1 mL, 3.22 mmol) and *N*,*N*′-diisopropylcarbodiimide (1 mL, 6.44 mmol) were reacted in hexane. A slight increase in the temperature was observed. After stirring for 24 h, evaporation of the solvent, and recrystallization from a hexane/diethyl ether mixture at −30 °C, colorless crystals suitable for X-ray single-crystal analysis were collected. Yield: 1.96 g (92% based on [Hf(NEtMe)$_4$]). Mp: 188 °C. Anal. Calcd for $C_{26}H_{60}N_8Hf$: C, 47.09; H, 9.12; N, 16.89. Found: C, 47.3; H, 9.12; N, 17.06. ^{1}H NMR (60 °C, 250 MHz, toluene-d_8): δ_H 0.94 (6H, triplet, Hf{(N^{i}Pr)$_2$C(N(CH$_2$C*H*$_3$)(Me)}), 1.23 (6H, triplet, Hf{N(CH$_2$C*H*$_3$)(Me)}), 1.30 (24H, doublet, Hf{(N(CH(C*H*$_3$)$_2$))$_2$C(NEtMe)}), 2.58 (6H, singlet, Hf{(N^{i}Pr)$_2$C(N(Et)(C*H*$_3$))}), 2.93 (4H, quartet, Hf{(N^{i}Pr)$_2$C(N(C*H*$_2$-CH$_3$)(Me)}), 3.34 (6H, singlet, Hf{N(Et)(C*H*$_3$)}), 3.67 (4H, quartet, Hf{N(C*H*$_2$CH$_3$)(Me)}), 3.80 (4H, septet, Hf{(N(C*H*(CH$_3$)$_2$))$_2$C(NEtMe)}). ^{13}C NMR (room temperature, 400 MHz, C_6D_6): δ_C 13.78 (Hf{(N^{i}Pr)$_2$C(N(CH$_2$C*H*$_3$)Me)}), 15.34 (Hf{N(CH$_2$C*H*$_3$)Me}), 24.45−26.45 (Hf{(N(CH(C*H*$_3$)$_2$))$_2$C(NEt$_2$)}), 36.90 (Hf{(N^{i}Pr)$_2$C(N(CH$_2$CH$_3$)C*H*$_3$)}), 41.45 (Hf{N(Et)C*H*$_3$}), 46.91 (Hf{(N^{i}Pr)$_2$C(N(C*H*$_2$CH$_3$)CH$_3$)}), 47.34 (Hf{(N(C*H*(CH$_3$)$_2$))$_2$C(NEtMe)}), 50.69 (Hf{N(C*H*$_2$CH$_3$)Me}), 171.97 (Hf{(N-^{i}Pr)$_2$C(N(CH$_2$CH$_3$)CH$_3$)}).

Synthesis of [Hf{η^2-(iPrN)$_2$CNMe$_2$}$_2$(NMe$_2$)$_2$] (3). This compound was prepared in a manner similar to that described for **1** by the reaction of [Hf(NMe$_2$)$_4$] (1.65 g, 4.65 mmol) with *N*,*N*′-diisopropylcarbodiimide (1.56 mL, 10 mmol) in 30 mL of hexane. The product was isolated as colorless crystals after recrystallization from hexane at −30 °C. Yield: 2.31 g (81% based on [Hf(NMe$_2$)$_4$]). Mp: 161 °C. Anal. Calcd for $C_{22}H_{52}N_8Hf$: C, 43.52; H, 8.63; N, 18.54. Found: C, 43.30; H, 8.21; N, 18.06. ^{1}H NMR (80 °C, 250 MHz, toluene-d_8): δ_H 1.23 (24H, doublet, Hf{(N(CH(C*H*$_3$)$_2$))$_2$C(NMe$_2$)}), 2.58 (12H, singlet, Hf{(N^{i}Pr)$_2$C(N(C*H*$_3$)$_2$)}), 3.28 (12H, singlet, Hf{N(C*H*$_3$)$_2$}), 3.77 (4H, septet, Hf{(N(C*H*(CH$_3$)$_2$))$_2$C(NMe$_2$)}). ^{13}C NMR (room temperature, 400 MHz, toluene-d_8): δ_C 23.75−26.76 (Hf{(N(CH(C*H*$_3$)$_2$))$_2$C(NMe$_2$)}), 40.10 (Hf{(N^{i}Pr)$_2$C(N(C*H*$_3$)$_2$)}, Hf{N(C*H*$_3$)$_2$}), 47.46 (Hf{(N(C*H*(CH$_3$)$_2$))$_2$C(NMe$_2$)}), 171.70 (Hf{(N^{i}Pr)$_2$C(N(Me$_3$)$_2$)}).

Synthesis of [{μ_2-NC(NMe$_2$)$_2$}{NC(NMe$_2$)$_2$}$_2$HfCl]$_2$ (4). In a 100-mL flask, 1.01 mL of 1,1,3,3-tetramethylguanidine (8 mmol) was dissolved in 20 mL of diethyl ether. To this solution was added at −50 °C 5 mL of *n*-butyllithium (1.6 M solution in *n*-hexane, 8 mmol), and the reaction mixture was allowed to stir for a period of 2 h. A white precipitate was formed, and the whole suspension was added to another suspension of $HfCl_4$ (0.85 g, 2.67 mmol) in toluene (30 mL). The mixture was refluxed for 24 h. After filtration, the solvent was removed in vacuo and the crude product was collected as a microcrystalline white powder. The solid was dissolved in hexane and left to recrystallize at room temperature over a period of 2 days. Yield: 0.59 g (77% based on $HfCl_4$). Mp: 174 °C. Anal. Calcd for $C_{30}H_{72}N_{18}Hf_2Cl_2$: C, 32.38; H, 6.52; N, 22.65. Found: C, 32.94; H, 6.31; N, 22.78. ^{1}H NMR (room temperature, 250 MHz, toluene-d_8): δ_H 2.79 (24H, singlet, Hf{(NC(N(C*H*$_3$)$_2$)$_2$)}), 2.99 (12H, singlet, Hf{η_2-(NC(N(C*H*$_3$)$_2$)$_2$)}). ^{13}C NMR (room temperature, 250 MHz, toluene-d_8): δ_C 41.52 (Hf{(NC(N(C*H*$_3$)$_2$)$_2$)}), 42.06 (Hf{μ_2-(NC(N(C*H*$_3$)$_2$)$_2$)}), 157.95 (Hf{(NC(N(CH$_3$)$_2$)$_2$)}).

Structural Determination for Compounds 1−4. Single crystals of compounds **1**−**4** were mounted on thin glass capillaries and then cooled to the data collection temperature (150 K). Diffraction data were collected on a X-calibur 2 Oxford diffractometer using graphite-monochromated Mo Kα radiation (λ = 0.710 73 Å). The structure was solved using the *SHELXL-97* software package and refined by full-matrix least-squares methods based on F^2 with all observed reflections. Crystal data and final agreement factors are listed in Table 1.

Thin Film Deposition and Characterization. As an example, preliminary CVD experiments were performed using compound **2** as the precursor, employing a home-built, horizontal cold-wall, low-pressure CVD reactor.[42] N_2 (flow rate: 50 sccm) and O_2 (flow rate: 50 sccm) were used as carrier and reactive gases, respectively. For each deposition, approximately 200 mg of the fresh precursor was filled into a glass bubbler in a glovebox. The substrate temperature was varied between 300 and 700 °C, while the precursor vaporizer was maintained at 120 °C. Depositions were carried out for 60 min, and the reactor pressure was maintained at 1 mbar. Single-crystal p-type Si(100) substrates (1 cm × 1 cm), which were precleaned using standard methods, were used for film deposition. The native oxide was not removed prior to deposition. The crystallinity of the films was investigated by X-ray diffraction (XRD) analyses using a Bruker D8 Advance AXS diffractometer [Cu Kα radiation (1.5418 Å)] with a position-sensitive detector. All films were analyzed in the $\theta-2\theta$ geometry. The surface morphology of the film was analyzed by scanning electron microscopy (SEM) using a LEO Gemini SEM 1530 electron microscope. An Oxford ISIS EDX system coupled to the SEM instrument was used for the energy-dispersive X-ray (EDX) analysis. Atomic force microscopy (AFM) using a nanoscope multimode III AFM (Digital Instruments) instrument in contact mode was employed. Rutherford backscattering (RBS) measurements (to determine the film thickness and composition) were carried out with a 2-MeV He beam of the Dynamitron-Tandem accelerator in Bochum with beam intensities of about 10 nA. A silicon surface barrier detector with an energy resolution of 15 keV was placed at an angle of 170° with respect to the beam axis. The

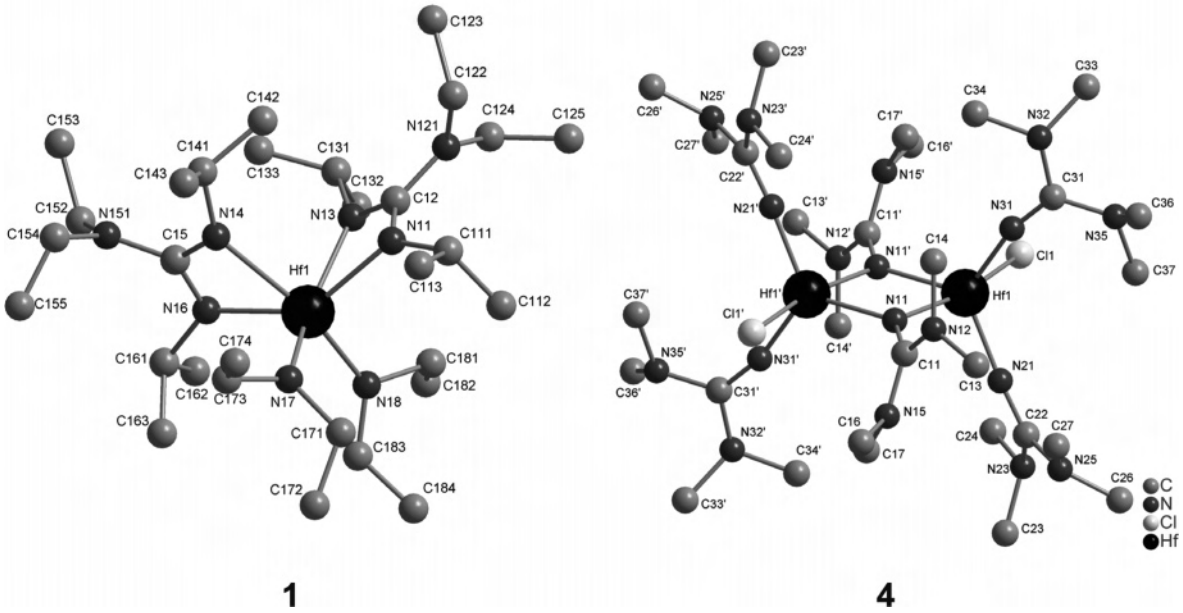

Figure 1. Crystal structures of **1** and **4**.

spectra were analyzed with the program *RBX* using the stopping powers of the program *SRIM*. The thin films were profiled using sputtered neutral mass spectrometry (SNMS) on a VG SIMSLABB IIIA instrument [MATS (U.K.) Ltd.]. The primary ion beam was Ar at 10 keV, usually operated at high currents (0.8−1.0 μA) over large areas (0.5−4-mm raster size) depending on the total depth requirements. For electrical measurements, Pt electrode pads were sputter-deposited on top of the HfO_2 films and patterned using shadow masks or lift-off lithography. Capacitance−voltage curves were obtained with a HP 4284 LCR meter using a frequency of 100 kHz.

Results and Discussion

As a part of our interest in the coordination chemistry of all-N Hf complexes, we attempted the reaction of 2 equiv of *N*,*N*-diisopropylcarbodiimide with $[Hf(NR_2)_4]$, (where R_2 = Et_2, Et and Me, or Me_2). The reactions were carried out at ambient temperature in hexane, which resulted in the formation of mixed amido/guanidinatohafnium(IV) complexes **1**−**3**. The reactions are illustrated in Scheme 2(i).

The synthesis of **1**−**3** follows a relatively easy insertion reaction wherein two of the labile amide moieties replaced from the primary ligand sphere of the metal are inserted on the central C atoms of the two *N*,*N*′-diisopropylcarbodiimide ligands, leading to the formation of monomeric bis(dialkylamido)bis(guanidinato)hafnium(IV) complexes. Upon an increase in the molar ratio to 3:1 or 4:1, the formation of tris- and/or tetrakis(guanidinato)hafnium complexes was not observed, possibly because of the larger steric demand of the diisopropylguanidinate ligands.

Consequently, less sterically hindered 1,1,3,3-tetramethylguanidine was investigated as the ligand for the synthesis of the tetrakis(guanidinato)hafnium complex. As described before, a salt metathesis reaction between $HfCl_4$ and $[LiNC(NMe_2)_2]_2$ resulted in the formation of the dimeric complex **4**, where at each Hf center only three of the chloride moieties are substituted by guanidinates. Our efforts in substituting the fourth chloride moiety by increasing the molar ratio of the ligand were unsuccessful and could most likely be due to the increased sterical demand of the ligand sphere around the metal center. Further attempts to exchange chloride by the less-demanding dimethylamido or azido groups were also unsuccessful. The presence of Cl in the molecule and the dimeric structure of the molecule make complex **4** less interesting as a possible precursor for MOCVD of HfO_2 thin films. Hence, the solid-state structure and NMR spectra of **4** will be discussed briefly.

The solid-state structures of compounds **1** and **4** are presented in Figure 1, and selected bond lengths and angles for **1**−**4** are given in Table 2. The coordination geometry around the Hf center in **1**−**3** could be described as a distorted octahedron, where the metal center is surrounded by four N atoms of the *cis*-guanidinato ligands and a further two of the dialkylamido groups, completing its coordination sphere. Compounds **1**−**3** carry similar crystallographic features, and therefore the crystal structure of one of the representative compounds (**1**) is described in detail.

To evaluate the degree of distortion of **1**, it is reasonable to consider the planes formed by N17, N11, N13, Hf1 and N18, N16, N14, Hf1 with a calculated average deviation of the atoms out of the corresponding planes in the range of 0.05 Å. For an ideal octahedron, the angles in each of the two orthogonal planes should be 90°, 90°, and 180°, respectively (Figure 2).

Although, in the case of complexes **1**−**3**, significant deviations from the ideal octahedral geometry were observed (Table 2), it is interesting to note that the difference in angles N11−Hf1−N13 and N16−Hf1−N14 [58.6(3)° for both] is about 32°. Thus, the major angular distortion could be associated with the small bite angles of the chelating guanidinate ligands.[30,43] Additional factors for the high distortion of the molecular geometry could be the presence of the four bulky isopropyl groups, which induce a large

Table 2. Selected Bond Lengths (Å) and Angles (deg) for Complexes **1**−**4**

1		**2**		**3**		**4**	
Hf1−N17	2.081(9)	Hf1−N4	2.065(13)	Hf1−N18	2.075(4)	Hf1−N21	1.997(5)
Hf1−N18	2.082(11)	Hf1−N3	2.104(13)	Hf1−N17	2.081(4)	Hf1−N31	2.003(5)
Hf1−N16	2.196(8)	Hf1−N23	2.192(12)	Hf1−N16	2.204(4)	Hf1−N11	2.144(5)
Hf1−N11	2.227(9)	Hf1−N11	2.212(12)	Hf1−N11	2.207(4)	Hf1−N11	2.162(5)
Hf1−N13	2.331(9)	Hf1−N21	2.331(12)	Hf1−N13	2.286(4)	Hf1−C11	2.5218(16)
Hf1−N14	2.341(9)	Hf1−N13	2.348(12)	Hf1−N14	2.310(4)	N11−C11	1.312(8)
N11−C12	1.315(13)	N11−C12	1.36(2)	N13−C12	1.317(6)	N21−C22	1.282(8)
C12−N13	1.319(13)	N12−C12	1.37(2)	N11−C12	1.334(7)	N31−C31	1.259(8)
C12−N121	1.405(15)	C12−N13	1.35(2)	N12−C12	1.393(7)	C11−N12	1.363(8)
N14−C15	1.333(14)	N21−C22	1.328(18)	N14−C15	1.327(6)	C22−N23	1.410(8)
C15−N16	1.337(14)	N22−C22	1.401(19)	N15−C15	1.388(6)	C31−N32	1.405(8)
C15−N151	1.392(14)	C22−N23	1.339(18)	N16−C15	1.352(6)		
N16−Hf1−N14	58.6(3)	N11−Hf1−N13	59.4(4)	N11−Hf1−N13	58.63(15)	Hf1−N11−Hf1	102.8(2)
N18−Hf1−N16	102.8(4)	N3−Hf1−N11	100.6(5)	N18−Hf1−N11	102.44(16)	C11−N11−Hf1	126.3(4)
N18−Hf1−N14	161.3(3)	N3−Hf1−N13	160.0(5)	N18−Hf1−N13	160.73(15)	C22−N21−Hf1	174.2(5)
N11−Hf1−N13	58.6(3)	N23−Hf1−N21	58.7(4)	N16−Hf1−N14	58.97(14)	C31−N31−Hf1	166.2(5)
N17−Hf1−N11	102.3(3)	N4−Hf1−N23	100.2(5)	N17−Hf1−N16	102.89(16)	N12−C11−N15	114.9(6)
N17−Hf1−N13	160.6(3)	N4−Hf1−N21	158.8(5)	N17−Hf1−N14	161.76(14)	N25−C22−N23	112.6(5)

geometry distortion in order to minimize the repulsions between these groups.

Another interesting feature in complexes **1**−**3** is the significant difference between the Hf−N bond lengths of the guanidinate N atoms trans to the NR_2 groups, which indicates the presence of a strong π-donating effect (trans effect) of the dialkylamido groups. In addition to the planarity of these NR_2 groups, the sum of the bonding angles around N17, N18 (**1**), N3, N4 (**2**), and N17, N18 (**3**) is almost 360°, pointing to the sp^2 hybridization of the N centers attached to the metal. Although such a phenomenon was observed in the case of related zirconium guanidinate complexes containing π-donating chloride ligands,[30,43] analogous hafnium amidinate and guanidinate complexes did not show such an effect.[30,44]

The question regarding the conjugation of the p orbital of the NR_2 center with the π system of the NCN moiety in the guanidinate ligand and the particular contributions of the resonance forms (Scheme 1) could be discussed considering two parameters. In the case of a significant conjugation, the NR_2 function should be sp^2-hybridized, allowing the donation of the lone pair localized on the nonhybridized p orbital into the NCN electronic system. In addition, there should be a minimal torsion angle between the plane of the NR_2 function and that defined by the NCN chelate for optimal π-orbital overlap. As revealed from the single-crystal X-ray analysis, the corresponding guanidinate NR_2 functions of compounds **1**−**3** are almost planar with dihedral angles between 167° and 177°. In addition to this, the sum of the bonding angles around the respective N atoms is almost 360°, pointing to the particular sp^2 hybridization of these N centers. The torsion angles between the plane NR_2 functions and the NCN moieties for the guanidinate ligands in **1**−**3** are 48−49°, pointing to the fact that only a reduced $\pi-\pi$ interaction between the exocyclic N and the NCN chelate is taking place. Thus, the corresponding structures of the guanidinate ligands in **1**−**3** can be rationalized between the limiting forms of sp^3- or sp^2-hybridized N of the CNR_2 functions (Scheme 1).

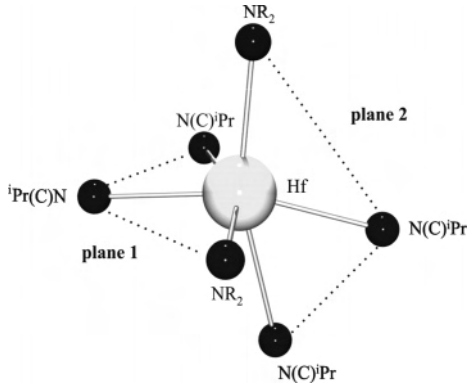

Figure 2. Coordination sphere of Hf in **1**−**3** composed of two orthogonal planes.

In contrast to compounds **1**−**3**, the single-crystal X-ray analysis of complex **4** revealed a dimeric structure (Figure 1). The molecule exhibits a planar Hf_2N_2 ring with two guanidinato groups bridging the Hf centers via imido N atoms. Thus, the coordination geometry around each of the quasi-five-coordinated, fully symmetrical metal centers could be described as trigonal bipyramidal. As expected, because of their position between two strong Lewis acidic centers, the Hf1−N11 (2.144 Å) and N11−C11 (1.312 Å) bond lengths of the bridging guanidinato ligands are significantly longer than those of the guanidinates bonded to only one of the metal centers. Additionally, a clear shortening of C11−N12 and C11−N15 bond lengths, when compared to the other C−NMe_2 bond lengths, could be observed. Thus, all of the N atoms of the bridging guanidinato ligands could be considered to possess interstitial sp^2 character, whereas in the guanidinates bonded to only one metal, a clear difference between the imido sp N and amido sp^3 N atoms could be made. As expected, complex **4** exhibits a simple ^{1}H NMR, which consists of only two singlets with an intensity ratio of 2:1 and thus confirms the C_2 symmetry of its dimeric structure. The signal at 2.79 ppm corresponds to the methyl groups of the singly bonded guanidinate ligands and the one at 2.99 ppm to the methyl groups of the bridging ligands.

NMR Studies of 1−**3.** The room-temperature ^{1}H NMR spectra of **1**−**3** show a complex solution behavior, resulting

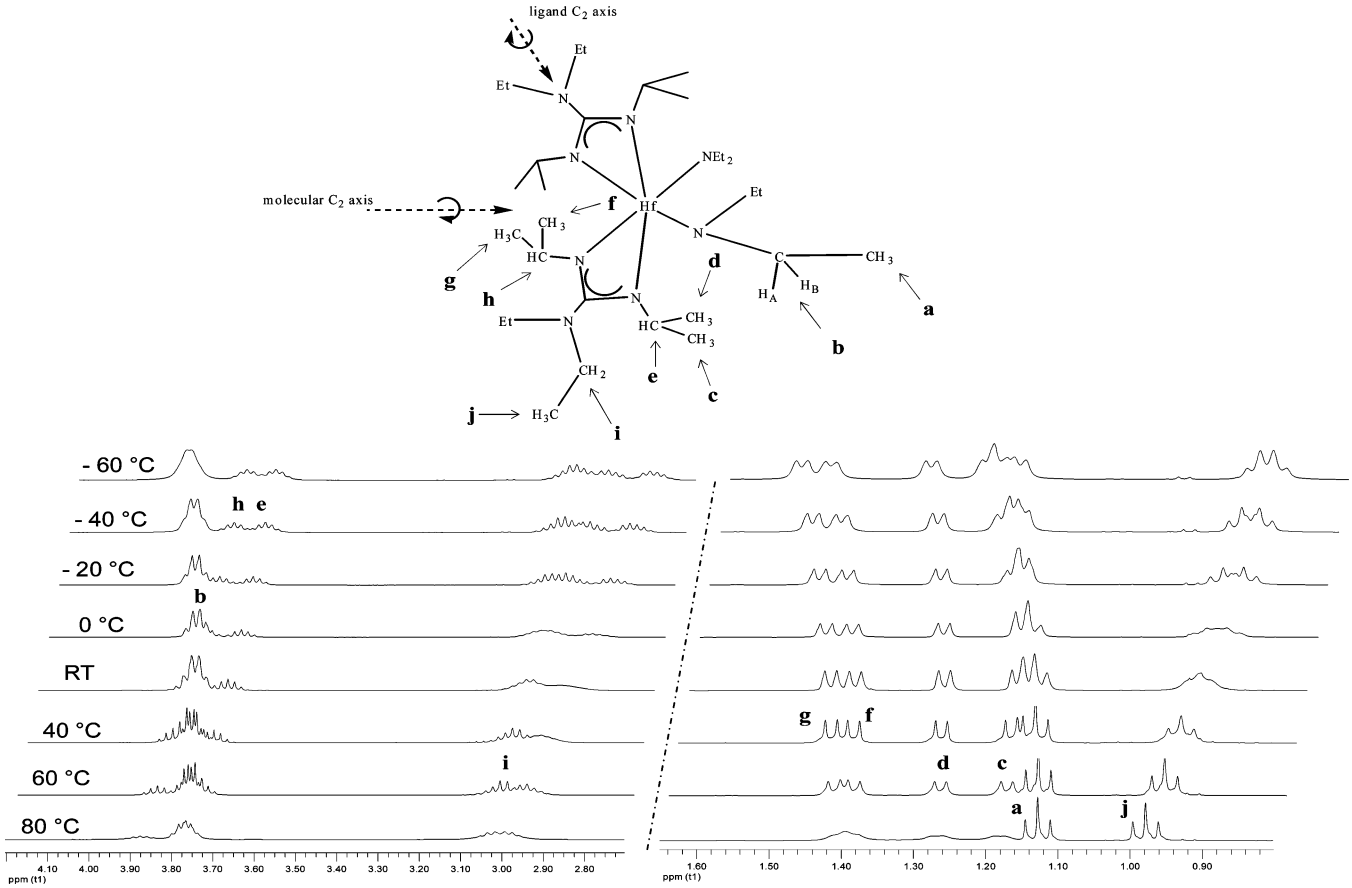

Figure 3. Temperature-dependent ^{1}H NMR spectra of complex **1** (toluene-d_8, 250 MHz).

in an onset of broad resonances especially significant in the case of **2** and **3** (see the Supporting Information). For complex **1**, a broad resonance centered at 0.94 ppm (**j**) can be assigned to the methyl group of the NEt_2 moiety bonded to the guanidinate ligand (Figure 3).

The splitting of this resonance at temperatures between −60 and −20 °C corresponds to a hindered rotation of this group around the $(^iPrN)_2C-N$ axis (due to the sp^2 character of the N atom as well as the sterical repulsion between the NEt_2 group and the ^{i}Pr rests), which is slow at the NMR time scale. At higher temperatures (40−80 °C), this process became faster at the NMR time scale and the broad resonance turns into a sharp triplet (**j**). The quartet at 1.18 ppm observed at room temperature could only be assigned based on the spectra recorded at 40 and 60 °C. They show a low-field shift of a doublet, which can be assigned to one of the isopropyl methyl groups (**c**). This separates it from the triplet corresponding to the methyl group of the NEt_2 attached to the metal (**a**). The methylene group coupled to this methyl is assigned to one of the multiplets found at around 3.7−3.8 ppm (**b**). Also the methylene group of NEt_2 bonded to the guanidinato moiety displays a multiplet at 2.9−3.0 ppm (**i**). The protons of all CH_2 groups are diastereotopic, thus giving four different doublets of quartets. The CH groups of the ^{i}Pr groups give rise to four doublets (1.18, 1.27, 1.39, and 1.42 ppm at 60 °C). This is evidently due to the steric interaction between the diethylamido group and the guanidinato ligands, which even in solution forces the molecule into a distorted geometry in which the isopropyl groups are not equivalent on the NMR time scale.

The observation that the eight isopropyl methyl groups of **1** give rise to only four doublets at temperatures from −60 to +60 °C is explained by the C_2 symmetry of the molecule in solution, which is consistent with the symmetry observed in the solid state (Figure 1). Because of this symmetry, the two guanidinate ligands are magnetically equivalent at all temperatures. In addition, a possible reason for the broad resonances in the isopropyl methyl region (1.1−1.5 ppm) at 80 °C could be the presence of two fluxional processes: a racemization of **1** combined with rotation of the guanidinate ligand around its internal C_2 axis, observed in related guanidinate and amidinate complexes.[44,45] For the correct assignment of all of the peaks of compound **1** at room temperature, two-dimensional (2D) heteronuclear multiple-quantum coherence (HMQC) spectra were recorded (see the Supporting Information).

The ^{1}H NMR spectrum of **2** at room temperature exhibits one set of broad resonances, indicating much stronger fluxional behavior when compared to the spectrum of **1** (see the Supporting Information). This observation is consistent with a lower activation barrier for the guanidinate ligand rotation and racemization, caused by the decreased sterical demand of the ethylmethylamido groups in **2**. Even at temperatures as low as −60 °C, the fluxional processes are still taking place, resulting in the formation of distinct but still broad resonances. Upon heating of **2** to 80 °C in toluene-

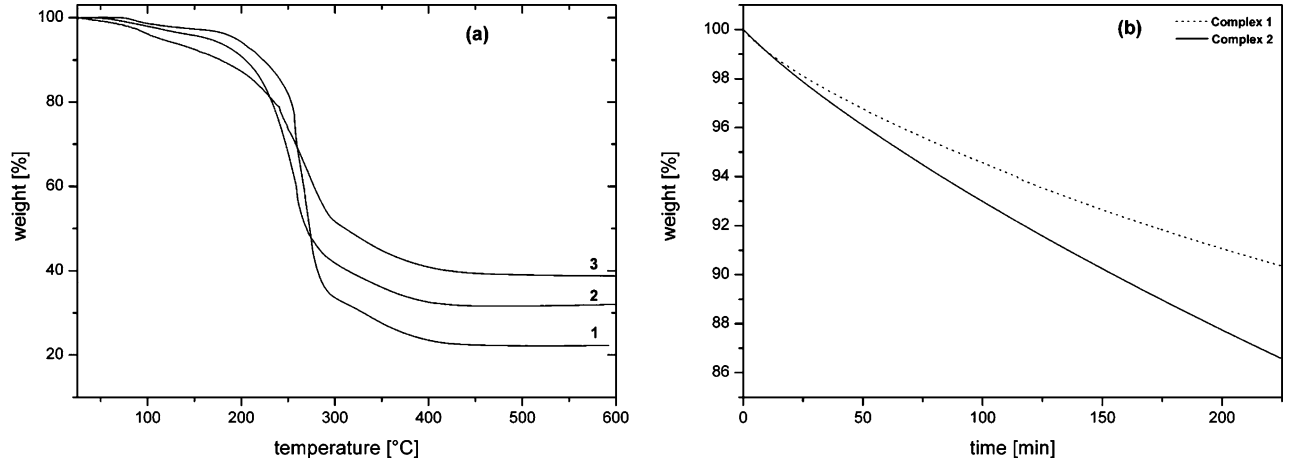

Figure 4. (a) TGA curves for complexes **1**−**3**. (b) Isothermal studies of **1** and **2** at 120 °C.

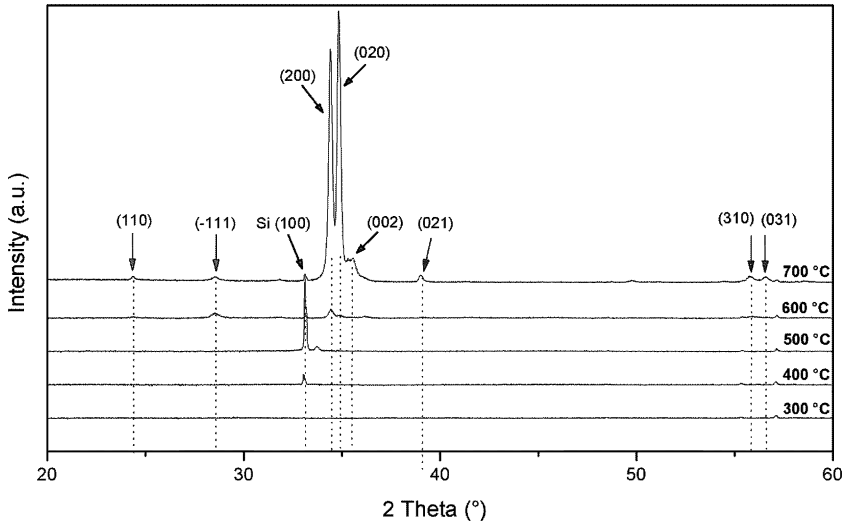

Figure 5. XRD patterns of HfO_2 films grown at temperatures between 300 and 700 °C using complex **2**.

d_8, fast exchange is observed. At this temperature, only one doublet and one septet are observed for the isopropyl methyl (**d**) and methyne (**e**) resonances, respectively. Because of the fast exchange, the diastereotopic CH_2 groups of the ethylmethylamido moieties give rise to two quartets (**b** and **f**) instead of the expected two doublets of quartets, as observed in compound **1**. The two single resonances at 2.58 and 3.34 ppm were assigned to the methyl groups (**c** and **h**). The ^{1}H NMR spectra of **3** are similar to those of **2** discussed above and are presented in the Supporting Information.

Thermal Analysis. Prior to thin film deposition, complexes **1**−**3** were evaluated by thermogravimetric analysis (TGA) for their suitability as CVD precursors. The TGA curves of complexes **1**−**3** are shown in Figure 4a, which reveals that complexes **1**−**3** sublime above 80 °C. There is a sufficient window between sublimation and decomposition (>200 °C), which renders them suitable for vapor deposition techniques.

In a CVD process where the precursor is a solid, the sublimation of a precursor is rather important because the constant sublimation rate during deposition can ensure a constant precursor mass transport. Therefore, we carried out isothermal studies at different temperatures to study the sublimation behavior. Figure 4b shows examples of isothermal curves (at ambient pressure) at 120 °C for complexes **1** and **2**, which show constant weight loss of these compounds over a long period of time (>200 min) that is desirable for CVD purposes. From the slopes of the curves, the sublimation rate of compound **2** was slightly higher than of **1** at 120 °C, and therefore as a part of our initial screening process for HfO_2 thin film deposition, we used compound **2** as the CVD precursor.

MOCVD of HfO_2 Thin Films. The MOCVD experiments were performed using a low-pressure, horizontal cold-wall reactor. Using compound **2**, it was possible to grow HfO_2 thin films at temperatures as low as 300 °C using O_2 as the oxidant. HfO_2 thin films with thicknesses in the range of 100−1620 nm were grown on Si(100) substrates in the temperature range of 300−700 °C, and the corresponding growth rates were on the order of 2−27 nm/min (see the Supporting Information, Table 1).

XRDs were recorded to deduce the onset of crystallization, and the results are shown in Figure 5. The films grown at low temperatures (300−500 °C) were amorphous and begin to crystallize at 600 °C (Figure 5). With an increase in the substrate temperature, the crystallization proceeds through an intermediate tetragonal and mixed phase (600 °C) to the finally stable monoclinic phase of HfO_2 at temperatures

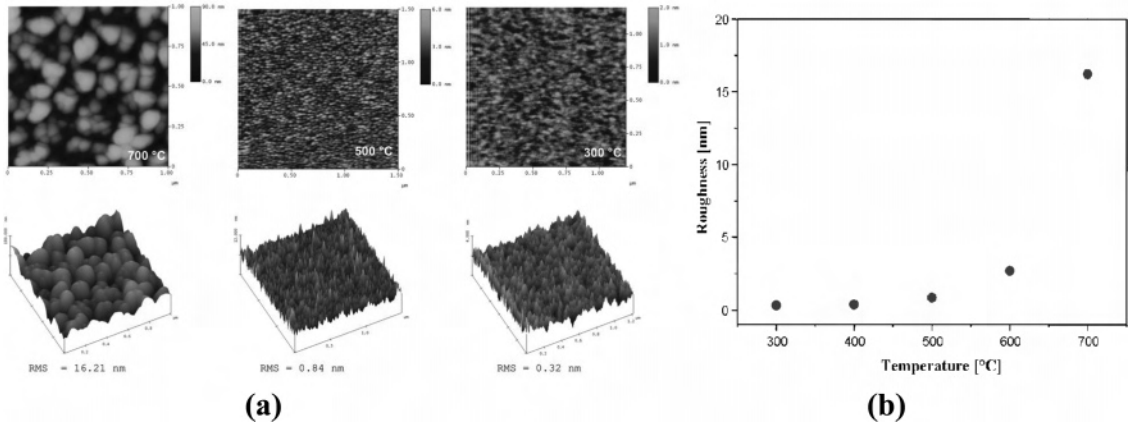

Figure 6. (a) Representative AFM images (2D and 3D) and (b) rms roughness of HfO_2 films deposited on Si(100) as a function of the substrate temperature using complex **2**.

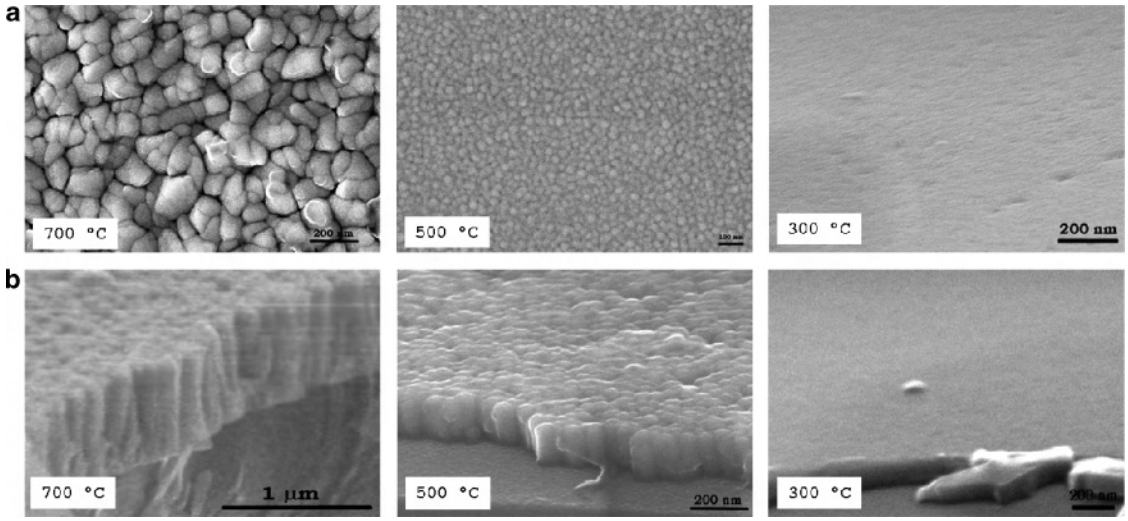

Figure 7. (a) SEM images of as-deposited HfO_2 films on Si(100) grown at different substrate temperatures using complex **2** (above) and (b) SEM cross-sectional view of the corresponding films (below).

above 700 °C. From the application point of view, amorphous dielectric films provide an improved barrier to dopant diffusion relative to that in polycrystalline films where diffusion occurs at the grain boundaries. The possibility of depositing amorphous films over a wide temperature range (300−500 °C) using dialkylamido/guanidinato complex **2** could be an added advantage.

The surface morphology of the HfO_2 films was studied using AFM and SEM analysis. Figure 6a shows the AFM micrographs (2D and 3D) of films obtained from compound **2**, while Figure 6b summarizes the root-mean-square (rms) roughness of the films as a function of the deposition temperature.

The films were smooth over the deposition temperature range of 300−500 °C, with the rms roughness in the range of 0.32 (film thickness = 110 nm) to 0.84 nm (film thickness = 265 nm), respectively. There is significant change in the rms roughness at the transition temperature from amorphous to crystalline films observed above 600 °C, e.g., from rms = 2.5 nm at 600 °C (film thickness = 940 nm) to rms = 16.2 nm at 700 °C (film thickness = 1620 nm) (Figure 6a,b). The higher average rms roughness for crystalline films with increasing thickness might be attributed to grain growth at higher temperatures. The progressive grain growth as a function of substrate temperatures is clearly seen from the SEM analysis, which is illustrated in Figure 7. The film grown at 300 °C did not show any surface features due to the amorphous phase. As the temperature is increased to 500 °C, microcrystalline grains are formed, which are uniformly distributed. The SEM cross-sectional image of the films grown at 500 and 700 °C indicates a columnar growth (Figure 7b).

The presence of Hf and O in the films was confirmed by EDX (Figure 8). The composition and thickness of the films were determined by RBS spectroscopy. The HfO_2 films grown in the temperature range of 300−500 °C were stoichiometric (the stoichiometric ratio of Hf/O was found to be 1:1.9 to 1:2; Table 1 in the Supporting Information). RBS analysis carried out on a HfO_2 film grown at 500 °C on a Si(100) substrate from compound **2** is depicted in Figure 9. The spectrum revealed the signals from Hf as well as from O in the layer, and the experimental curve fitted well with the simulated curve.

To determine the in-depth composition of the films, secondary SNMS analysis was performed on a 60-nm-thick HfO_2 film (Figure 10). Apart from Hf and O in the bulk of

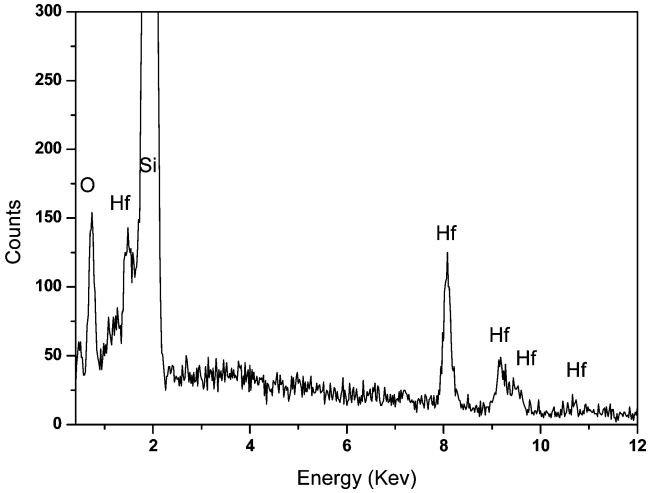

Figure 8. EDX spectrum of an HfO_2 film grown on Si(100) at 500 °C using complex **2**.

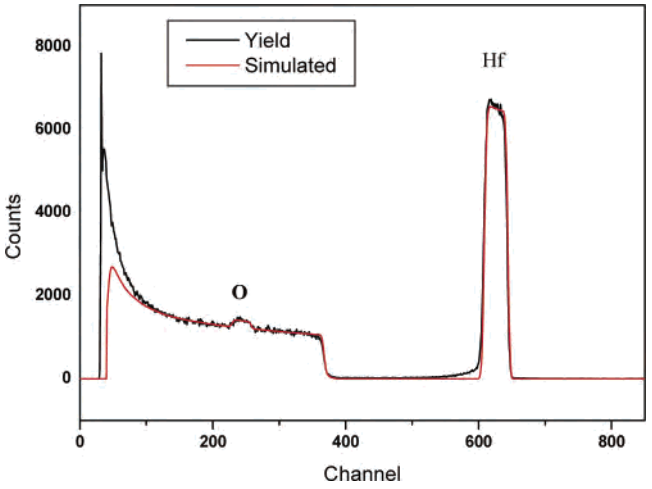

Figure 9. RBS spectrum of an HfO_2 film grown on Si(100) at 500 °C using complex **2**.

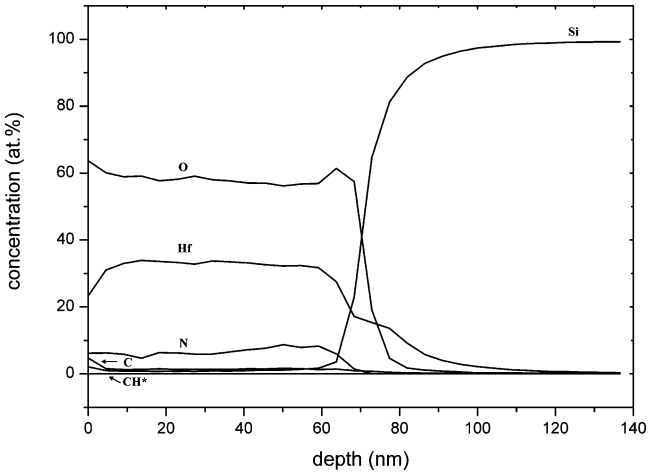

Figure 10. SNMS spectrum of an HfO_2 film (ca. 60 nm) grown at 600 °C using complex **2**.

the film, interestingly some content of N was also detected (ca. 7%). As seen in the spectra, the constant N/Hf signal ratio throughout the film indicates a uniform distribution of N. This is in contrast to literature reports, where the N content of the HfO_2 films deposited at low temperatures from different dialkylamides is about 1−4% and decreases with an increasing deposition temperature.[46−48] It could be expected that the increased N content in the films deposited using complex **2** could improve their thermal stability and resistance to O and dopant diffusion. Further detailed investigations are warranted to study the incorporation of N as a function of the film growth temperature.

The slight increase of the N content in the depth range from 50 to 60 nm could be due to the crystallinity of the film. In crystallized films, N atoms can readily diffuse along the grain boundaries and accumulate at the interface between the high-*k* film and the silicon substrate.[49] The depth profile shows a 4 atom % C contamination on the surface, which decreases to 1.5 atom % in the first few nanometers and remains constant within the film. The level of C incorporation is lower than the results published for HfO_2 deposited using different dialkylamide precursors, where the C contamination was relatively higher.[46−48] Besides O and Si, Hf and N are also detected in the interfacial layer (depth 65−75 nm), suggesting a nitrided hafnium silicate layer formation. The electrical properties of the HfO_2/Si films were studied in terms of the capacitance−voltage characteristics to investigate their suitability for application in Pt/HfO_2/SiO_x/Si capacitor structures (see the Supporting Information). The calculated dielectric constant from the capacitance at accumulation of the HfO_2 film deposited at 500 °C was $k \sim 24$. Detailed electrical investigations are currently underway.

In summary, the synthesis and characterization of novel guanidinate-stabilized amide complexes of Hf, showing potential as molecular precursors for MOCVD of HfO_2, are reported. Compounds **1**−**3** are monomers, and compound **4** is a dimer, linked together via bridged guanidinate ligands. The compounds are much less sensitive to air and moisture compared to the parent hafnium alkylamides. The thermal characteristics show a quantitative and unchanged volatilization at the operating temperature in a MOCVD process. Compound **2** has been tested for the growth of HfO_2 thin films by MOCVD, which yielded smooth, uniform, stoichiometric HfO_2 thin films at relatively low deposition temperatures, which is an important figure of merit. The SNMS data indicated that HfO_2 films obtained from compound **2** have lesser C and higher N content than the parent alkylamide compounds. The higher level of N incorporation in HfO_2 thin films obtained from guanidinate-based Hf precursors is interesting and warrants further studies. The preliminary electrical results open intriguing perspectives for gate oxide applications of the obtained films. Because of the good thermal stability and reactivity, guanidinate-based Hf complexes are quite interesting for ALD of HfO_2 thin films. In addition, these complexes are highly soluble in organic solvents and can be used in LI-MOCVD. We are currently investigating the use of guanidinate-based Hf complexes in

(47) Williams, P. A.; Jones, A. C.; N, L. T.; Chalker, P. R.; Taylor, S.; Marshall, P. A.; Bickley, J. F.; Smith, L. M.; Davies, H. O.; Critchlow, G. W. *Chem. Vap. Deposition* **2003**, *9* (6), 309.
(48) Ohshita, Y.; Ogura, A.; Hoshino, A.; Hiiro, S.; Machida, H. *J. Cryst. Growth* **2001**, *233*, 292.
(49) Lee, C.; Choi, J.; Cho, M.; Park, J.; Hwang, C. S.; Kim, H. J.; Jeong, J. *J. Vac. Sci. Technol. B* **2004**, *7*, F18.

industrial tool reactors for ALD (F-120, ASM) and LI-MOCVD (AIX 2600G3 planetary reactor) applications.

Acknowledgment. The authors acknowledge the financial support from the Deutsche Forschungsgemeinschaft (Grants DFG, CVD-SPP-1119, and DE-790/3-3) and Prof. R. A. Fischer for his continuous support. A.M. thanks the German Academic Exchange Service (DAAD) for a fellowship.

Supporting Information Available: X-ray crystallographic data (CIF), crystal structures and temperature-dependent ^{1}H NMR spectra of complexes **2** and **3**, 2D HMQC spectra of complexes **1** and **2**, capacitance−voltage characteristics of the Pt/HfO_2/SiO_x/Si capacitors, and RBS analysis of HfO_2 films grown from **2**. This material is available free of charge via the Internet at http://pubs.acs.org.

IC061056I